IEEE Photonics Journal
An IEEE Photonics Society Publication

Open Access

On-Chip Low-Power Gray Code Generation Based on Opto-Mechanical Microring Resonators

Volume 12, Number 3, June 2020

Li Liu
Yue Yang
Jin Yue
Shasha Liao

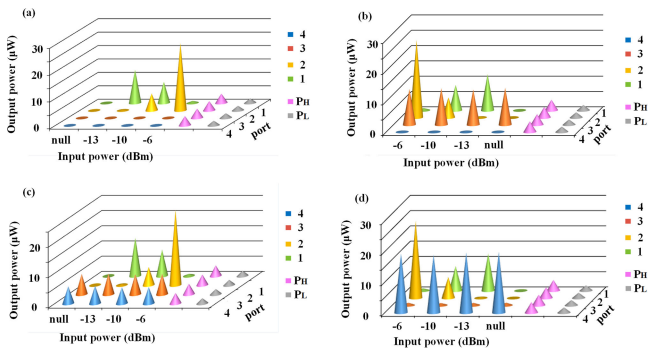

DOI: 10.1109/JPHOT.2020.2986188

On-Chip Low-Power Gray Code Generation Based on Opto-Mechanical Microring Resonators

Li Liu [1], Yue Yang [2], Jin Yue,[1] and Shasha Liao [2]

[1]School of Automation, China University of Geosciences, Wuhan 430074, China
[2]Hubei Key Laboratory of Advanced Control and Intelligent Automation for Complex Systems, Wuhan 430074, China
[3]Wuhan National Laboratory for Optoelectronics School of Optical and Electrical Information, Huazhong University of Science and Technology, Wuhan 430074, China
[4]The Key Lab of Mobile Communication Technology, Chongqing University of Posts and Telecommunication, Chongqing 400065, China

DOI:10.1109/JPHOT.2020.2986188

Manuscript received February 19, 2020; accepted April 3, 2020. Date of publication April 10, 2020; date of current version May 13, 2020. This work was supported in part by the National Natural Science Foundation of China under Grants 61805215 and 61801063, in part by Wuhan Municipal Science and Technology Bureau under Grant 2019010701011410, and in part by Engineering Research Center of Mobile Communications, Ministry of Education. Corresponding author: Li Liu (e-mail: liliu@cug.edu.cn).

Abstract: We propose and experimentally demonstrate on-chip energy-efficient Gray code generation based on a scalable and compact optical encoder. The operation principle of the integrated encoder is based on the nonlinear effects in silicon opto-mechanical microring resonators (MRRs), which could be excited by ultra-low input powers. By adjusting the input powers with hierarchical power levels, the red-shifts of the MRR transmission spectrum could be flexibly manipulated. In this case, the output powers of the MRR drop-port and through-port could be controllable and switchable to generate different codes. Through tuning the optical encoding powers in a specific rule, 4-bit and 2-bit Gray codes have been successfully demonstrated. The required power of the proposed 4-bit encoder is as low as −6 dBm, which is favorable to build energy-efficient optical encoding systems. To the best of our knowledge, we have realized a nano-mechanical optical encoder with the lowest required power. Moreover, the encoder structure has great scalability, thus 2N-bit Gray code could be generated by utilizing 2N-1 add-drop MRRs. With the dominant advantages of ultra-low power consumption (−6 dBm), compact size (0.08 mm^2) and great scalability, the proposed optical encoder has many significant applications in optical encoding and communication chips.

Index Terms: Optical encoder, opto-mechanical microring resonator, low-power, great extendibility.

1. Introduction

Optical logic gates and logic functional devices are fundamental components and long-standing goals in optical communication systems [1]–[3]. Especially, with advantages of low latency transmission, parallel processing and high stability, reliable optical encoders are key devices to guarantee high communication performances in long-haul signal transmissions [4]. To date, optical encoders have been realized by photonic crystals [5], fractional Talbot effect [6] and point-source light-emitting diodes [7]. Among the various optical encoders, one important encoding type is

Gray code which shows the dominant advantages of minimization error and convenience [8]. Moreover, with remarkable features of a cycle and single-step switching, Gray code could effectively reduce the data operations and economize the system power consumption [9]. Nowadays, Gray code has attracted widespread attention and is widely used in digital processing systems [10], such as fiber-optic localization [11], optical communication networks [12] and image processing [13]. Different optical encoding methods of Gray code have been demonstrated by using discrete devices, such as utilizing the electro-optic effect in the Mach–Zehnder interferometer [14] and cross gain modulation (XGM) in semiconductor optical amplifiers (SOAs) [15]. However, the required powers of most optical encoders are higher than 20 dBm which limit their practical applications. Recently, to pursue better integration and reliability of optical encoding systems, researchers focus on silicon-on-insulator (SOI) technology due to its advantages of low-loss and low-cost [16]–[20]. Unfortunately, there are few research efforts on optical Gray code generation by exploiting silicon devices. In order to break the above limitation, more efficient and low-power mechanisms for optical Gray code generation are highly desired.

In the past decade, opto-mechanical devices have attracted increasing interests as for the ability to effectively combine the two significant fields of nanophotonics and nano-mechanics [21], [22]. Especially in the compact opto-mechanical microring resonators (MRRs), the nonlinear effects (mainly including the opto-mechanical effect and thermo-optic effect) could be significantly activated by low input powers. Due to the enhanced gradient of the optical field, the opto-mechanical effect could be effectively excited in the free-hanging MRRs [23], [24]. On the other hand, the thermo-optic effect is also one key factor to induce the MRR resonance red-shifts [25]. As the removal of the oxide substrate could effectively decrease the device heatsink, the temperature rise of the opto-mechanical microring would be much higher. Therefore, the silicon opto-mechanical devices provide an effective solution for low-power optical processing.

In this paper, we experimentally demonstrate optical 4-bit and 2-bit Gray code generation based on the silicon opto-mechanical MRRs. The operation principle of the optical encoder is the nonlinear effects in the free-hanging microrings, whose transmission spectra could be flexibly manipulated by low optical powers. In this case, the output powers of the MRR drop-port and through-port could be switchable and controllable to generate different codes. The experimental results show that with injecting optical powers as low as -6 dBm, an optical encoder for 4-bit Gray code has been successfully achieved. To the best of our knowledge, the power consumption of the nano-mechanical optical encoder is the lowest among the integrated optical encoders. The proposed scheme provides an optical processing approach for Gray code generation with advantages of ultra-low power, compact footprint and great scalability, which is competent for practical applications in on-chip optical communication systems.

2. Operation Principle

The key device of the optical encoder is a silicon opto-mechanical add-drop MRR, as shown in Fig. 1(a). Half of the oxide substrate underneath the microring is removed, leaving the corresponding MRR arc to be free-hanging. The operation principle of the free-hanging MRR is based on the multiple nonlinear effects, mainly including the thermo-optic (TO) effect and opto-mechanical effect, which are analyzed in our previous work [16]. The resonance red-shift of the MRR is proportional to the input power P_{in}. Namely, the MRR spectrum could be manipulated by adjusting the input optical powers.

The drop-port (Port 1) and through-port (Port 2) of the MRR correspond to the high-bit and low-bit of 2-bit Gray code, respectively. The output powers (P_{out}) of Port 1 and Port 2 are written as P_1 and P_2, respectively. According to the encoding rules in communication systems, two threshold powers (high threshold power P_H and low threshold power P_L) are set to determine the output codes of bit "1" or bit "0". As shown in Eq. (1), the output code is defined as bit "1" if P_{out} is higher than P_H. In contrast, if P_{out} is lower than P_L, the output code is defined as bit "0".

$$\text{code} = 1(P_{out} > P_H); \text{code} = 0(P_{out} < P_L) \quad (1)$$

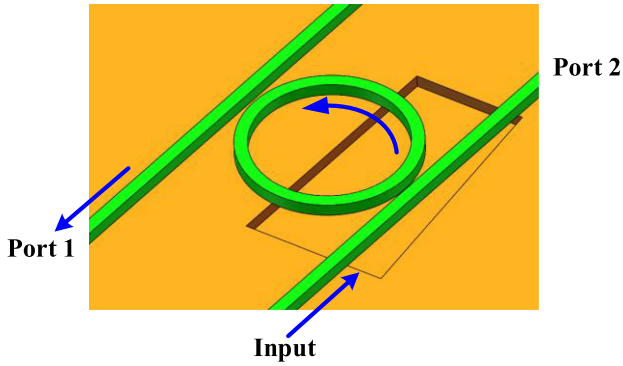

Fig. 1. The add-drop free-hanging MRR.

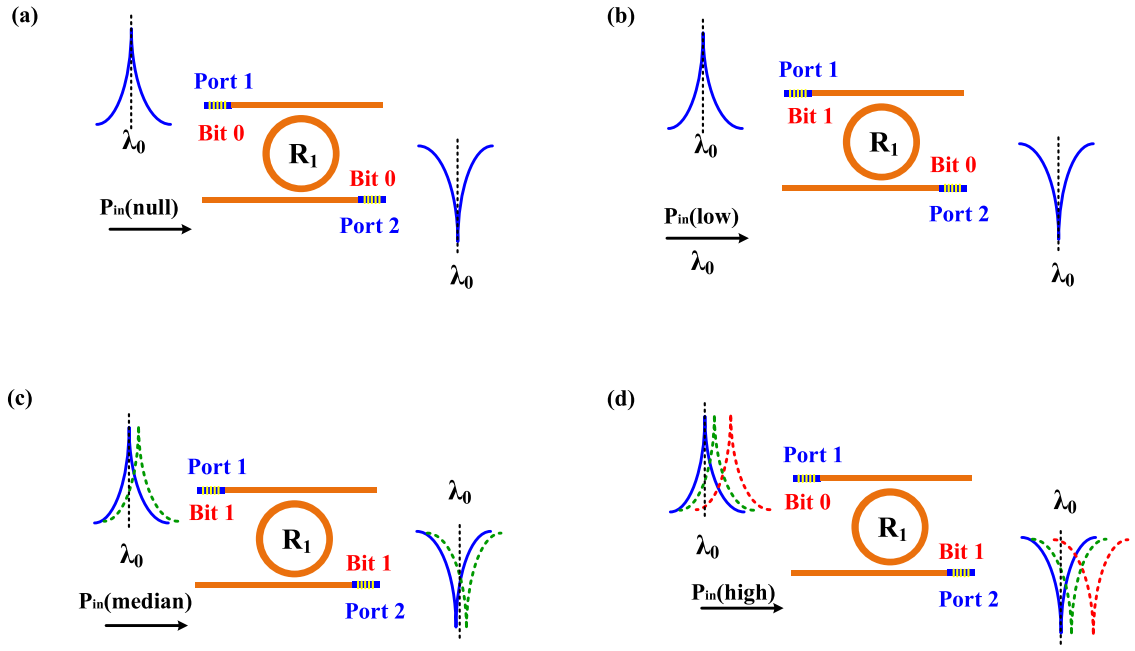

Fig. 2. Tuning process of the opto-mechanical MRR. The input power levels are (a) null, (b) low, (c) median, and (d) high, respectively.

The initial transmission spectra of the MRR are shown as the blue solid lines in Fig. 2(a) and the wavelength of the input light is fixed at the MRR initial resonance of λ_0. The detailed encoding process of 2-bit Gray code is described as follows. Firstly (Step 1), the input power at λ_0 is set at the level of "null" (i.e., no input power), hence there are definitely no output powers at Port 2 and Port 1. In this case, the output 2-bit code of Port 2 and Port 1 is bits "00", as shown in Fig. 2(a). Secondly (Step 2), the input power at λ_0 is increased to the level of "low" which is not high enough to affect the MRR (i.e., no resonance red-shift), as shown in Fig. 2(b). The major input power would transmit to Port 1. Namely, the output power P_2 is still lower than P_L to maintain Port 2 of bit "0" while the output power P_1 becomes larger than P_H to change Port 1 of bit "1". Therefore, the output 2-bit code turns into bits "01". Thirdly (Step 3), the light power at λ_0 is enhanced to the level of "median" in order to cause a medium spectrum red-shift, shown as the green lines in Fig. 2(c). In this case, the input power would be divided into two parts and transmit to the corresponding port. The two output powers are both higher than P_H, namely the output 2-bit code changes to bits "11". Finally (Step 4), the light power at λ_0 with the level of "high" is injected into the device, the MRR

TABLE 1
Encoding Rule for the 2-Bit Gray Code

Tuning process (4 steps)	Input power (λ_0)	Bit (Port 2)	Bit (Port 1)	2-bit Gray code
Step 1	null	0	0	00
Step 2	low	0	1	01
Step 3	median	1	1	11
Step 4	high	1	0	10

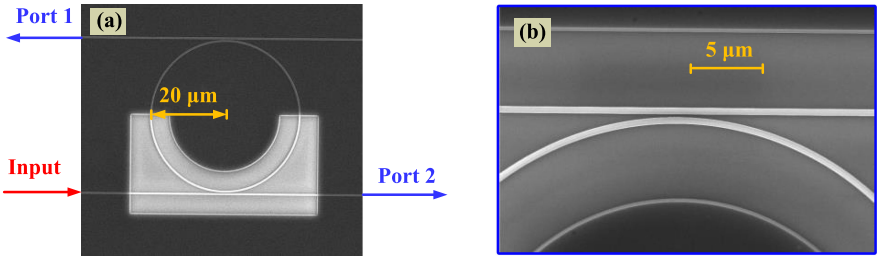

Fig. 3. SEM images of (a) the add-drop opto-mechanical MRR and (b) zoom in coupling region.

would experience a large enough resonance red-shift, shown as the red lines in Fig. 2(d). Thus the major light power could not couple into the MRR but transmits straight to Port 2. Namely, there is almost no output power at Port 1. In this case, the output 2-bit code switches to bits "10". Therefore, as shown in Table 1, the optical 2-bit Gray code could be generated by injecting resonance powers in the order of "null", "low", "median" and "high".

The add-drop opto-mechanical MRR is fabricated on a commercial SOI wafer whose silicon slab and buried oxide layer are 220 nm and 2 μm respectively. The MRR free-hanging arc is released by selective etching processing of three steps. Firstly, the whole MRR is transferred to the photoresist through E-beam lithography (EBL) and then etched downwards for 190 nm by inductively coupled plasma (ICP). Secondly, half of the MRR was patterned by a second EBL and etched downwards for another 30 nm to form a corrosion window. In this case, oxide substrate (SiO_2) around above half MRR would be exposed to the air while the other half MRR arc has 30 nm-thick silicon slab layer to protect this fixed structure from later corrosion of hydrofluoric (HF) acid. Finally, HF acid solution was utilized to selectively undercut the oxide substrate of the corrosion window, leaving the corresponding MRR arc to be free-hanging. Fig. 3(a) illustrates the scanning electron microscope (SEM) image of the opto-mechanical MRR. The MRR radius is 20 μm and the waveguide width is 450 nm. The zoom-in coupling region of the free-hanging structure is shown in Fig. 3(b). The effective index of the straight waveguide, the ridge MRR and the free-hanging MRR at 1550 nm are 2.33, 2.36 and 2.26, respectively. Namely, the waveguide effective index differences could be negligible, which benefits the signal transmission and coupling between different structures.

A low-power amplified spontaneous emission (ASE) source is coupled with a resonance continuous-wave (CW) light and injected into the silicon device in order to characterize the transmission spectrum. In the case of no input CW light, the initial MRR transmission spectra with resonance wavelength λ_0 of 1557.596 nm are shown as the pink lines in Fig. 4. The extinction ratios of the MRR through-port and drop-port are approximately 18 dB and 31 dB, respectively. To investigate the nonlinear effects in the free-hanging MRR, CW light with different powers are injected into the microring. With increasing the CW light powers in the order of -10.8 dBm, -7.6 dBm and -3.9 dBm, the spectrum red-shifts of the MRR [through-port in Fig. 4(a) and drop-port in Fig. 4(b)] are 0.015 nm (green solid line), 0.036 nm (red dashed line) and 0.08 nm (blue dash-dotted line), respectively.

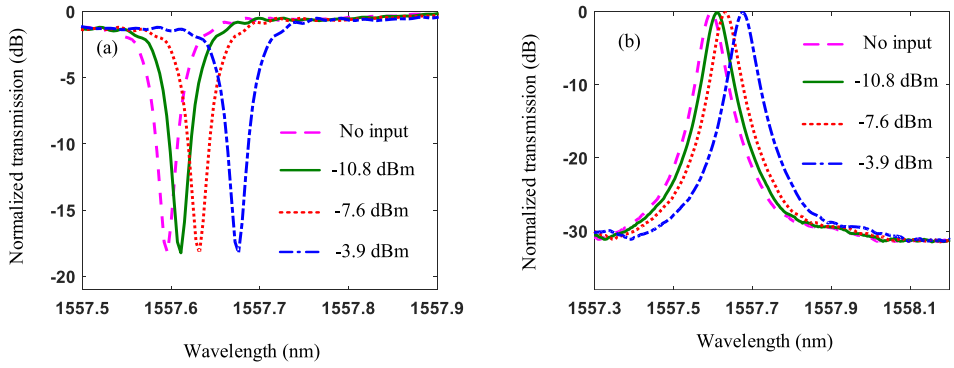

Fig. 4. With injecting different CW light powers, the transmission spectra of (a) MRR through-port and (b) drop-port, respectively.

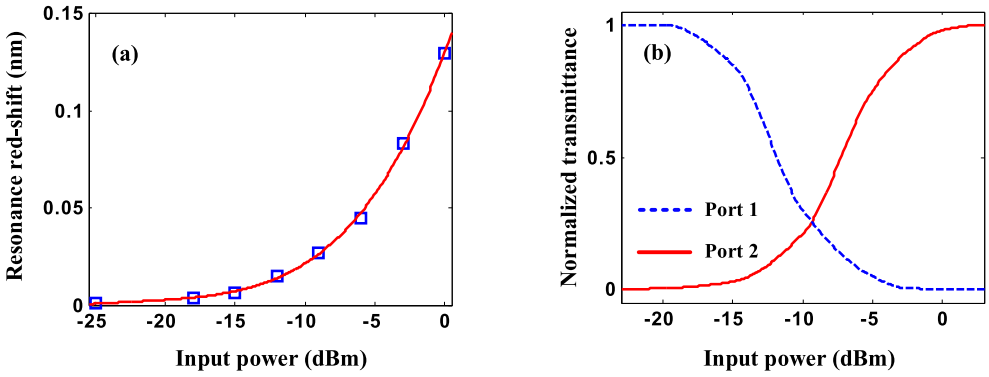

Fig. 5. (a) The MRR resonance red-shifts under different input powers. (b) Measured normalized transmittances of Port 1 (blue dotted line) and Port 2 (red solid line), respectively.

To further investigate the relationship between the resonance red-shifts and input powers, optical powers ranging from -25 dBm to 0 dBm in steps of 3 dBm are injected into the MRR, as shown in Fig. 5(a). For example, the red-shift could realize 0.13 nm when the input power is set as 0 dBm. In order to determine the input powers of "low", "median" and "high", the port normalized transmittances have been measured, as shown in Fig. 5(b). As discussed in Table 1, the four power levels of "null", "low", "median" and "high" are used to generate the 2-bit Gray code of "00", "01", "11" and "10", respectively. Therefore, according to the measured normalized transmittances in Fig. 5(b), the four power levels could be set to no input ("null"), -12 dBm ("low"), -9 dBm ("median") and -5 dBm ("high"), respectively.

3. Experimental Results

3.1 2-bit Gray Code Generation

The experimental configuration is shown in Fig. 6. The wavelength and output power of CW light emitted from the tunable laser sources (TLS) are fixed at λ_0 (i.e., 1557.596 nm). The input powers at λ_0 could be adjusted by a variable optical attenuator (VOA). Finally, power meter 1 and power meter 2 are used to measure the output powers at Port 1 (the low bit) and Port 2 (the high bit), respectively. Compared with the threshold powers (i.e., P_H and P_L), the 2-bit output codes could be achieved.

The histogram of the measured results is shown in Fig. 7. The output powers of the two ports are shown as the blue cuboids (Port 2) and the red cuboids (Port 1), respectively. In order to more intuitively illustrate the encoding results, the vertical coordinates are expressed by microwatt

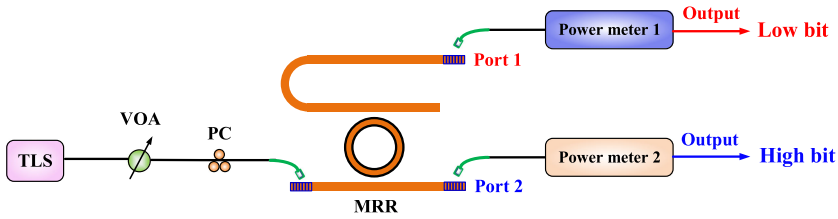

Fig. 6. Schematic diagram of the experimental setup. The components of the apparatus are labeled as follows: TLS, tunable laser source; VOA, variable optical attenuator; and PC, polarization controller.

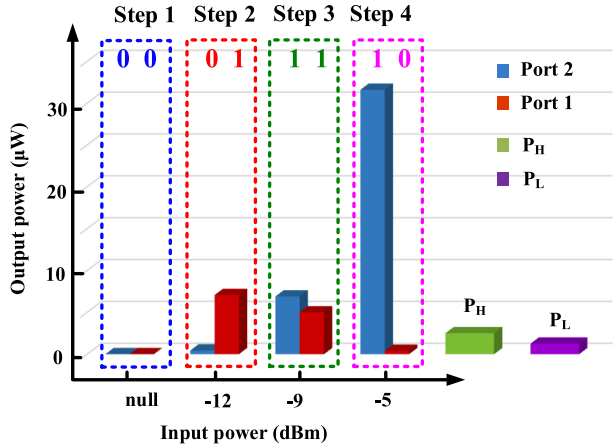

Fig. 7. Experimental encoding results of 2-bit Gray code with injecting powers in the order of "null", "low", "median", and "high".

(μW). The two threshold powers of P_H (green cuboids) and P_L (purple cuboids) are set as 2.5 μW (−26 dBm) and 1.25 μW (−29 dBm), respectively.

The detailed encoding process and results are described as follows. Firstly (Step 1), when there is no input power at λ_0 (i.e., power level of "null"), there are definitely no output powers at the two ports of the MRR. In this case, the output 2-bit Gray code is bits "00". Secondly (Step 2), the light power at λ_0 is set at −12 dBm (i.e., power level of "low") which is not strong enough to affect the MRR. The measured output powers are −33.5 dBm (Port 2) and −21.5 dBm (Port 1) to generate bits "01". Thirdly (Step 3), the light power at λ_0 is increased to −9 dBm (i.e., power level of "median") in order to induce a medium red-shift. In this case, the output powers of the two ports are −21.6 dBm (Port 2) and −23 dBm (Port 1), respectively. Thus the output code changes to bits "11". Finally (Step 4), the light power at λ_0 is enhanced to −5 dBm (i.e., the power level of "high") so as to cause a large enough red-shift of the MRR. The output powers of the two ports are −15 dBm (Port 2) and -34 dBm (Port 1), respectively. In this case, the output code turns into bits "10". Table 2 summarizes the measured output powers of λ_0 with the above four steps. With injecting light powers at λ_0 in the order of "null" (no power), "low" (−12 dBm), "median" (−9 dBm) and "high" (−5 dBm), an optical encoder to generate 2-bit Gray code with low-power has been successfully built.

3.2 4-bit Gray Code Generation

As one opto-mechanical MRR (or one resonance) could generate 2-bit Gray code, multi-bit Gray code encoder could be realized by multi-MRRs (or multi-resonances). As shown in Fig. 8, there are three cascaded opto-mechanical MRRs (i.e., R_1, R_2 and R_3). The resonance λ_1 of R_1 and the resonance λ_2 of R_2 in the encoding key region are utilized to generate 4-bit Gray code. The

TABLE 2
Measured Output Powers and Encoding Results under Different Input Powers

Tuning process (4 steps)	Input power (dBm) (λ_0)	Output power (dBm) (Port 2)	Output power (dBm) (Port 1)	2-bit Gray code
Step 1	null	null	null	00
Step 2	-12	-33.5	-21.5	01
Step 3	-9	-21.6	-23	11
Step 4	-5	-15	-34	10

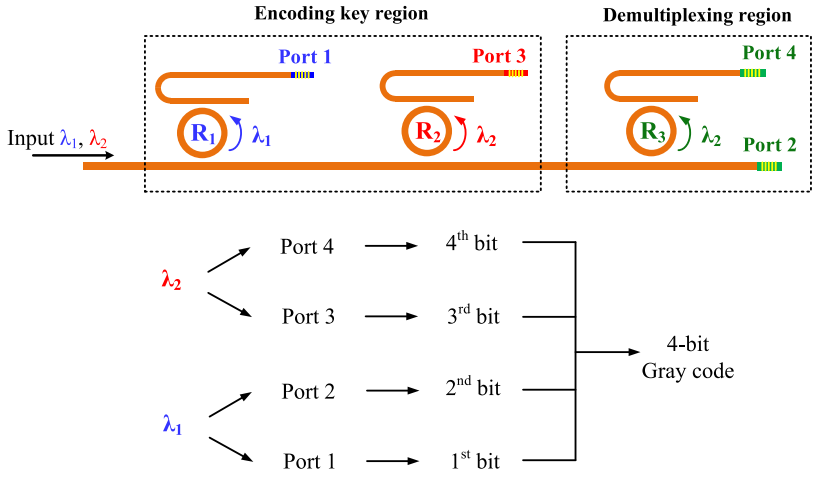

Fig. 8. Cascaded MRR structure for 4-bit Gray code generation.

resonance of R_3 in the demultiplexing region is around λ_2 in order to demultiplex the two resonant wavelengths. In this case, the output bits of Port 2 and Port 1 which corresponds to the 2nd-bit and 1st-bit are determined by the powers of the resonance λ_1. On the other hand, the 4th-bit and 3rd-bit corresponding to Port 4 and Port 3 are controlled by the powers of λ_2.

The encoding rule of the 4-bit Gray code with sixteen steps is shown in Table 3. The resonant powers of λ_1 and λ_2 are utilized to generate the lower two bits (2nd-bit and 1st-bit) and the higher two bits (4th-bit and 3rd-bit), respectively. As discussed in the 2-bit encoder, with injecting the optical power of λ_1 in an order of "null", "low", "median" and "high", the corresponding lower two bits (2nd-bit and 1st-bit) are "00", "01", "11" and "10" respectively, shown as the first four steps (steps 1–4). Then, the powers of λ_1 are decreased in the opposite order of "high", "median", "low" and "null" (steps 5–8), which accordingly generate the lower two bits of "10", "11", "01" and "00", respectively. In the next eight steps (steps 9–16), the variation rule of λ_1 is the same as the first eight steps (steps 1–8). On the other hand, the powers of λ_2 are also increased in the order of "null", "low", "median" and "high", but each power state lasts four steps. Therefore, by simultaneously manipulating the powers of λ_1 and λ_2 in a specific rule, 4-bit Gray code could be achieved.

Fig. 9 shows the SEM image of the cascaded opto-mechanical MRRs for 4-bit Gray code generation. The radii of the MRRs and the waveguide widths are around 20 μm and 450 nm, respectively. The 4-bit Gray code corresponds to the output bits of Port 1 (the drop port of R_1, 1st-bit), Port 2 (the through port of R_3, 2nd-bit), Port 3 (the drop port of R_2, 3rd-bit) and Port 4 (the drop port of R_3, 4th-bit), respectively. The encoding key region (R_1 and R_2) and demultiplexing region (R_3) are shown as the two white boxes.

The device measured transmission spectra are shown in Fig. 10. The blue line in Fig. 10(a) and the red line in Fig. 10(b) are the drop transmissions of R_1 (i.e., Port 1) and R_2 (i.e., Port 3),

TABLE 3
Encoding Rule for 4-Bit Gray Code

Tuning process (16 steps)	Input power (λ_2)	Input power (λ_1)	4th-Bit (Port 4)	3rd-Bit (Port 3)	2nd-Bit (Port 2)	1st-Bit (Port 1)	4-bit Gray code
Step 1	null	null	0	0	0	0	0000
Step 2	null	low	0	0	0	1	0001
Step 3	null	median	0	0	1	1	0011
Step 4	null	high	0	0	1	0	0010
Step 5	low	high	0	1	1	0	0110
Step 6	low	median	0	1	1	1	0111
Step 7	low	low	0	1	0	1	0101
Step 8	low	null	0	1	0	0	0100
Step 9	median	null	1	1	0	0	1100
Step 10	median	low	1	1	0	1	1101
Step 11	median	median	1	1	1	1	1111
Step 12	median	high	1	1	1	0	1110
Step 13	high	high	1	0	1	0	1010
Step 14	high	median	1	0	1	1	1011
Step 15	high	low	1	0	0	1	1001
Step 16	high	null	1	0	0	0	1000

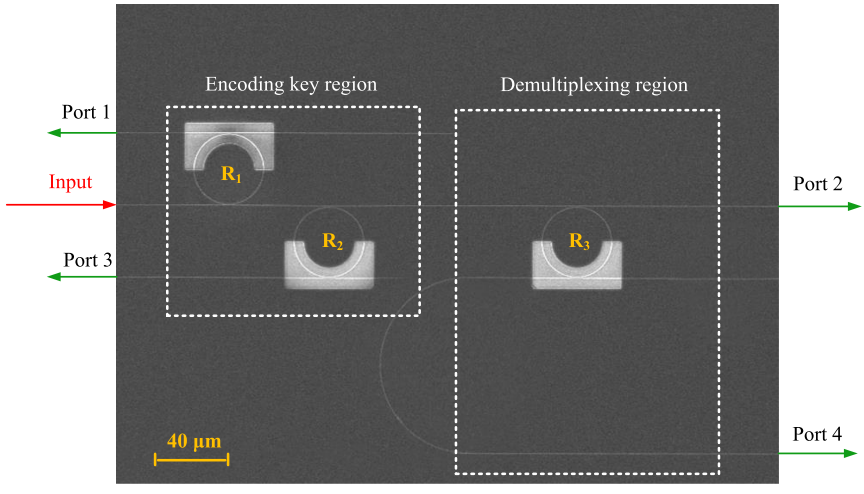

Fig. 9. SEM image of the 4-bit Gray code encoder.

respectively. It can be seen that the resonances λ_1 and λ_2 are around 1557.425 nm and 1555.62 nm respectively, which are absolutely separated. The extinction ratios of the two spectra are both larger than 30 dB. The transmission spectrum of Port 2 is shown in Fig. 10(c). The two notch wavelengths of the green curve are around 1555.62 nm and 1557.425 nm, and the corresponding extinction ratios are 26 dB and 16 dB. The drop transmission of R_3 is also measured which demonstrates the resonant wavelength of R_2 and R_3 are aligned around 1555.62 nm.

The experimental results of the 4-bit Gray code are shown in Fig. 11. The blue cone, red cone, yellow cone and green cone represent the output powers of Port 4, Port 3, Port 2 and Port 1, respectively. The two threshold powers denoted by the pink cone and grey cone are set as 3.5 μW (P_H) and 1.75 μW (P_L). The four input power levels of "null", "low", "median" and "high" are chosen as null, -13 dBm, -10 dBm and -6 dBm, respectively. Firstly, when there is no input power of λ_2

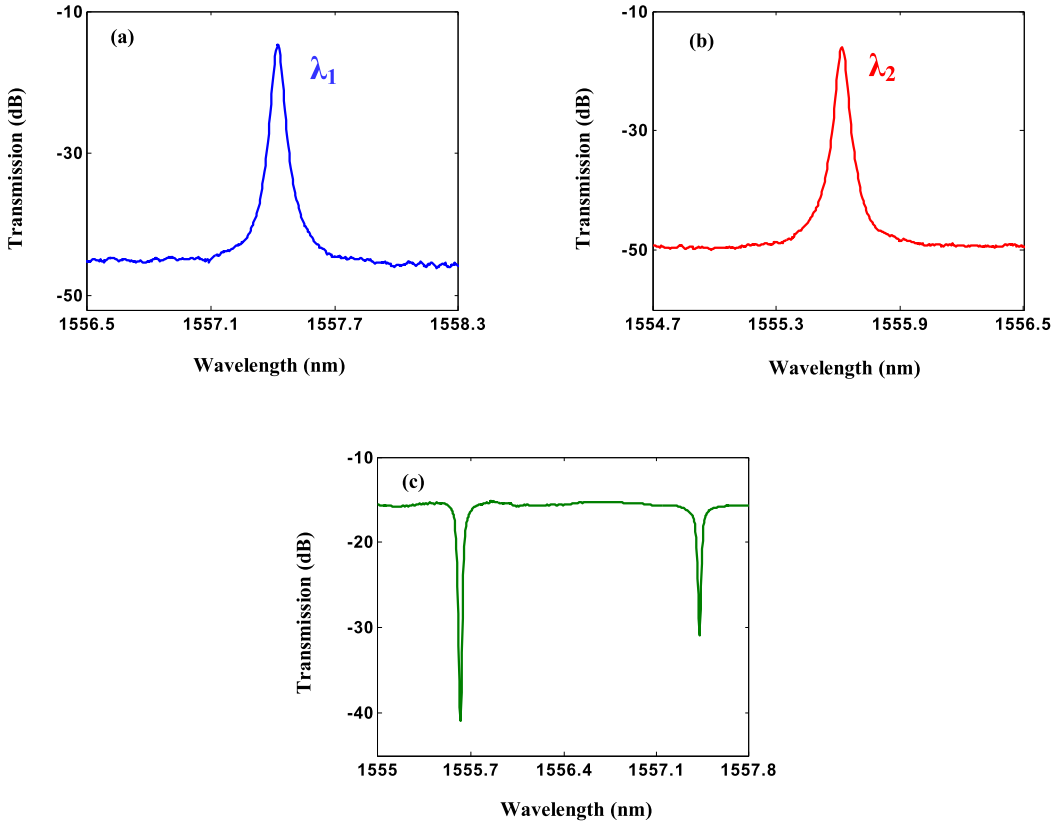

Fig. 10. The measured transmission spectra of (a) Port 1, (b) Port 3, and (c) Port 2, respectively.

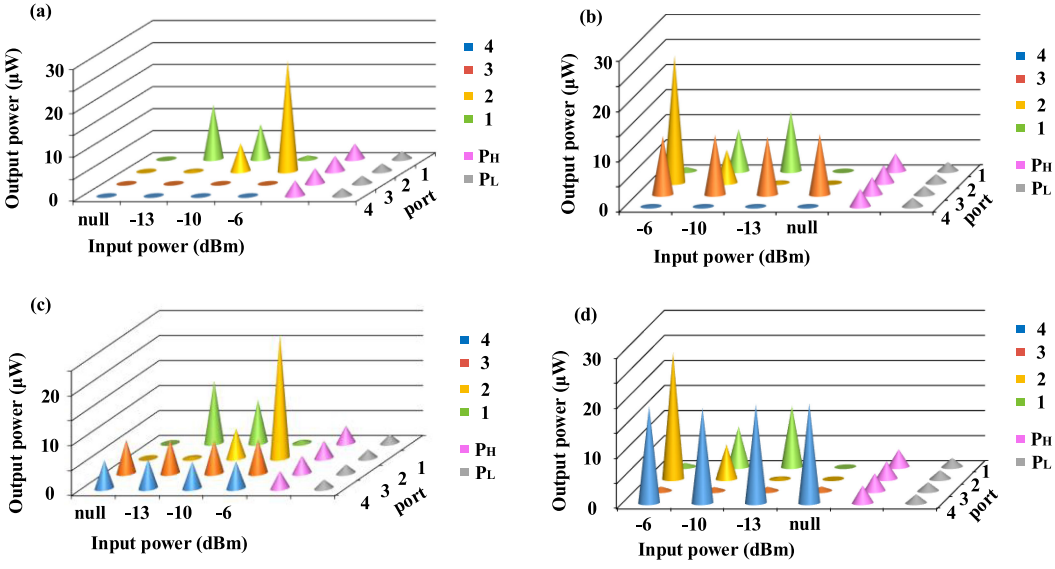

Fig. 11. The output powers of the four ports when the input powers of λ_2 are fixed at (a) null, (b) -13 dBm, (c) -10 dBm, and (d) -6 dBm, respectively. The pink and grey cones represent the threshold powers of P_H and P_L, respectively.

TABLE 4
Encoding Results for 4-bit Gray Code

Tuning process (16 steps)	Input power (dBm) (@ λ_2)	(@ λ_1)	Output power (μW) Port 4	Port 3	Port 2	Port 1	4-bit Gray code
Step 1	null	null	0	0	0	0	0000
Step 2	null	-13	0	0	0.32	12.36	0001
Step 3	null	-10	0	0	6.35	7.91	0011
Step 4	null	-6	0	0	25.13	0.78	0010
Step 5	-13	-6	0.21	11.65	25.32	0.76	0110
Step 6	-13	-10	0.18	11.89	6.58	8.32	0111
Step 7	-13	-13	0.25	11.52	0.43	11.87	0101
Step 8	-13	null	0.17	12.06	0	0	0100
Step 9	-10	null	5.68	6.75	0	0	1100
Step 10	-10	-13	5.87	6.86	0.37	12.53	1101
Step 11	-10	-10	5.39	6.68	5.96	8.65	1111
Step 12	-10	-6	5.43	6.79	24.81	0.68	1110
Step 13	-6	-6	19.32	0.83	25.28	0.79	1010
Step 14	-6	-10	18.96	0.75	6.87	8.06	1011
Step 15	-6	-13	19.67	0.81	0.45	12.18	1001
Step 16	-6	null	19.85	0.86	0	0	1000

TABLE 5
Performance Comparisons of Optical Encoders Using Nonlinear Effects

Nonlinear effect	Device	Optical power (dBm)
Cross-phase modulation [4]	Highly nonlinear fiber	30
Kerr effect [26]	Photonic crystal	29.8
Self-phase modulation [27]	Chalcogenide waveguide	> 30
Soliton self-frequency shift [28]	Highly nonlinear fiber	22.9
Free-carrier injection [29]	Silicon microring	14
This work (4-bit Gray code)	Silicon opto-mechanical MRRs	– 6

($P_{in}(\lambda_2)$ = "null"), the output 4-bit Gray codes are shown in Fig. 11(a). Because $P_{in}(\lambda_2)$ = null, the 4th-bit and 3rd-bit are certainly "00". As the input power of λ_1 varies in an order of null, -13 dBm, -10 dBm and -6 dBm, the 2nd-bit and 1st-bit are "00", "01", "11" and "10", respectively. Thus the corresponding output 4-bit Gray codes are "0000", "0001", "0011" and "0010", respectively. Secondly, the input power of λ_2 is enhanced to -13 dBm ($P_{in}(\lambda_2)$ = "low"). In this case, the generated 4-bit Gray codes are illustrated in Fig. 11(b). The 3rd-bit is changed to bit "1" while the 4th-bit maintains bit "0". When the input power $P_{in}(\lambda_1)$ is adjusted to -6 dBm, -10 dBm, -13 dBm and null in order, the 2nd-bit and 1st-bit are tuned as "10", "11", "01" and "00", respectively. In this case, the 4-bit Gray codes are "0110", "0111", "0101" and "0100". Thirdly, we increase the input power of λ_2 to -10 dBm ($P_{in}(\lambda_2)$ = "median"), so the 4th-bit and 3rd-bit are both changed to bit "1". The corresponding 4-bit Gray code is shown in Fig. 11(c). It can be seen that the output 4-bit Gray codes vary as "1100", "1101", "1111" and "1110" with adjusting $P_{in}(\lambda_1)$ of null, -13 dBm, -10 dBm and -6 dBm, respectively. Finally, Fig. 11(d) shows the output 4-bit Gray codes when $P_{in}(\lambda_2)$ is fixed at -6 dBm ($P_{in}(\lambda_2)$ = "high"). As $P_{in}(\lambda_1)$ is tuned as -6 dBm, -10 dBm, -13 dBm and null in order, the corresponding 4-bit Gray codes are "1010", "1011", "1001" and "1000", respectively. The measured output powers of the four ports are shown in Table 4. Therefore, 4-bit Gray codes have been experimentally achieved and the encoding rule is concise and regular.

Table 5 presents the experimental demonstrations of optical encoders using different nonlinear effects. The required encoding powers of most schemes are higher than 20 dBm, which limit their practical applications in optical communication systems. In contrast, by utilizing the nonlinear

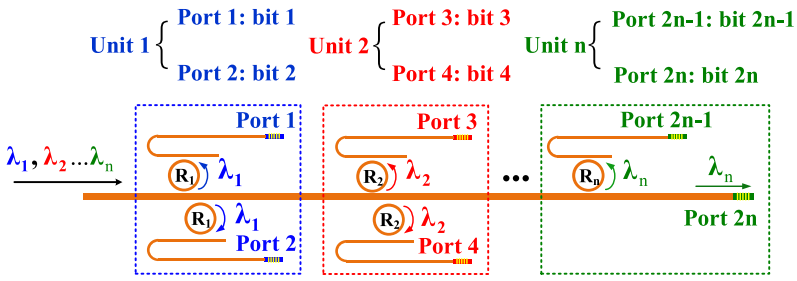

Fig. 12. The scalable topological structure of 2N-bit Gray code encoder.

effects in the opto-mechanical MRRs, the highest required power to generate 4-bit Gray code is as low as −6 dBm which is significant to build on-chip optical encoding systems with low-power consumption.

It should be noted that the proposed encoder is significant in optical multi-bit encoding chips with a competitive feature of the scalable topological structure, as shown in Fig. 12. The device basic unit is a group of two add-drop opto-mechanical MRRs with the same resonant wavelength. According to the encoding principle in Fig. 2, each unit could generate 2-bit Gray code. Therefore, 2N-bit Gray code could be achieved by combining N basic units (corresponding to 2N-1 MRRs) with different resonant wavelengths of λ_1, λ_2, ...λ_n. For example, by using Unit 1 (λ_1) and Unit 2 (λ_2), we have demonstrated 4-bit Gray code generation based on three cascaded MRRs. The major technical and engineering challenge of the scalable encoder is the wavelength alignment of each basic unit, which could be solved by the electrodes. Once one MRR of each basic unit is fabricated with electrodes, the two MRR resonances of every unit could be precisely aligned for 2-bit code generation. Another technical challenge is the crosstalk between different basic units, which could be also easily eliminated by optimizing the resonance intervals between different units. If the resonant peaks of λ_1, λ_2, ...λ_n do not overlap, the device crosstalk could be negligible.

In the future, the performance of the optical encoder could be improved by the following aspects. Firstly, the lengths of the free-hanging waveguides and the separation heights between the free-hanging arc and the oxide substrate could be optimized, in order to realize a much stronger opto-mechanical effect. Accordingly, the required powers would be reduced. Secondly, the coupling gaps between the MRRs and the straight waveguides could be finely designed to achieve higher Q factors. In this case, lower powers are required to excite the nonlinear effects in the opto-mechanical MRRs. Finally, by employing better fabrication technology and post-processing methods (e.g., thermal oxidation), the transmission loss of the MRRs could be significantly reduced [30] and then the required powers could be significantly decreased.

5. Conclusion

In conclusion, we have experimentally demonstrated an optical encoder for 4-bit and 2-bit Gray codes based on the nonlinear effects in silicon opto-mechanical MRRs. With the highest required powers as low as −6 dBm, three cascaded opto-mechanical MRRs are competent to generate 4-bit Gray code. Moreover, 2N-bit Gray code could be realized by utilizing 2N-1 add-drop MRRs. The scalable nano-mechanical optical encoder is significant to build on-chip low-power encoding and communication systems.

References

[1] X. Yang, X. Hu, H. Yang, and Q. Gong, "Ultracompact all-optical logic gates based on nonlinear plasmonic nanocavities," *Nanophotonics*, vol. 6, no. 1, pp. 365–376, 2017.
[2] A. E. Willner, S. Khaleghi, M. R. Chitgarha, and O. F. Yilmaz, "All-optical signal processing," *J. Lightwave Technol.*, vol. 32, no. 4, pp. 660–680, 2014.

[3] L. Liu, J. Dong, D. Gao, A. Zheng, and X. Zhang, "On-chip passive three-port circuit of all-optical ordered-route transmission," *Sci. Rep.*, vol. 5, 2015, Art. no. 10190.
[4] K. Ikeda, J. M. Abdul, S. Namiki, and K. I. Kitayama, "Optical quantizing and coding for ultrafast A/D conversion using nonlinear fiber-optic switches based on Sagnac interferometer," *Opt. Express*, vol. 13, no. 11, pp. 4296–4302, 2005.
[5] F. Mehdizadeh, M. Soroosh, H. Alipour-Banaei, and E. Farshidi, "Ultra-fast analog-to-digital converter based on a nonlinear triplexer and an optical coder with a photonic crystal structure," *Appl. Opt.*, vol. 56, no. 7, pp. 1799–1806, 2017.
[6] C. F. Kao and M. H. Lu, "Optical encoder based on the fractional Talbot effect," *Opt. Commun.*, vol. 250, no. 1, pp. 16–23, 2005.
[7] Y. Matsuzoe, K. Koizumi, T. Saitoh, and T. Yoshizawa, "Optimizing design of high-resolution optical encoder using a point-source light-emitting diode with slits," *Opt. Eng.*, vol. 44, no. 1, pp. 013609–013609, 2005.
[8] A. Kumar, and S. K. Raghuwanshi, "Implementation of optical gray code converter and even parity checker using the electro-optic effect in the Mach–Zehnder interferometer," *Opt. Quantum Electron.*, vol. 47, no. 7, pp. 2117–2140, 2015.
[9] J. S. Kim, J. G. Kim, H. Choi, and K. D. Seo, "Pixel-domain Wyner-Ziv residual video coder with adaptive binary-to-Gray code converting process," *Electron. Lett.*, vol. 49, no. 3, pp. 189–190, 2013.
[10] E. Agrell, J. Lassing, E.G. Storm, and T. Ottosson, "On the optimality of the binary reflected gray code," *IEEE Trans. Inform. Theory*, vol. 50, no. 12, pp. 3170–3182, 2004.
[11] J. C. Juarez, and H. F. Taylor, "Field test of a distributed fiber-optic intrusion sensor system for long perimeters," *Appl. Opt.*, vol. 46, no. 11, pp. 1968–1971, 2007.
[12] C. Kim and G. Li, "Direct-detection optical differential 8-level phase-shift keying (OD8PSK) for spectrally efficient transmission," *Opt. Express*, vol. 12, no. 15, pp. 3415–3421, 2004.
[13] J. M. Bueno and P. Artal, "Double-pass imaging polarimetry in the human eye," *Opt. Lett.*, vol. 24, no. 1, pp. 64–66, 1999.
[14] A. Kumar and S. K. Raghuwanshi, "Implementation of optical gray code converter and even parity checker using the electro-optic effect in the Mach–Zehnder interferometer," *Opt. Quantum Electron.*, vol. 47, no. 7, pp. 2117–2140, 2015.
[15] Y. J. Jung, S. Lee, and N. Park, "All-optical 4-bit gray code to binary coded decimal converter," in *Proc. Integr. Optoelectronic Devices (Soc. Photo-Opt. Instrum. Engineers)*, 2008, Art. no. 68900S.
[16] L. Liu, J. Yue, X. Fan, and W. Xue, "On-chip passive optical diode with low-power consumption," *Opt. Express*, vol. 26, no. 25, pp. 33463–33472, 2018.
[17] Y. Zhao, X. Wang, D. Gao, J. Dong, and X. Zhang, "On-chip programmable pulse processor employing cascaded MZI-MRR structure," *Frontiers Optoelectron.*, Vol. 12, pp. 148–156, 2019.
[18] L. Liu, J. Dong, and X. Zhang, "Chip-integrated all-optical 4-bit Gray code generation based on silicon microring resonators," *Opt. Express*, vol. 23, no. 16, pp. 21414–21423, 2015.
[19] X. Zhao *et al.*, "A nano-opto-mechanical pressure sensor via ring resonator," *Opt. Express*, vol. 20, no. 8, pp. 8535–8542, 2012.
[20] L. Liu, Y. Yang, Z. Li, X. Jin, W. Mo, and X. Liu, "Low power consumption and continuously tunable all-optical microwave filter based on an opto-mechanical microring resonator," *Opt. Express*, vol. 25, no. 2, pp. 960–971, 2017.
[21] Y. Huang, S. Zhu, H. Zhang, T. Y. Liow, and G. Q Lo, "CMOS compatible horizontal nanoplasmonic slot waveguides TE-pass polarizer on silicon-on-insulator platform," *Opt. Express*, vol. 21, no. 10, pp. 12790–12796, 2013.
[22] A. Einat, and U. Levy, "Analysis of the optical force in the micro ring resonator," *Opt. Express*, vol. 19, no. 21, pp. 20405–20419, 2011.
[23] C. Xiong, X. Sun, K. Y. Fong, and H. X. Tang, "Integrated high frequency aluminum nitride optomechanical resonators," *Appl. Phys. Lett.*, vol. 100, no. 17, 2012, Art. no. 171111.
[24] H. Qiu, J. Dong, L. Liu, and X. Zhang, "Energy-efficient on-chip optical diode based on the optomechanical effect," *Opt. Express*, vol. 25, no. 8, pp. 8975–8985, 2017.
[25] L. Liu *et al.*, "Low-power all-optical microwave filter with tunable central frequency and bandwidth based on cascaded opto-mechanical microring resonators," *Opt. Express*, vol. 25, no. 15, pp. 17329–17342, 2017.
[26] B. Youssefi, M. K. Moravvej-Farshi, and N. Granpayeh, "Two bit all-optical analog-to-digital converter based on nonlinear Kerr effect in 2D photonic crystals," *Opt. Commun.*, vol. 285, no. 13, pp. 3228–3233, 2012.
[27] R. Pant, C. Xiong, S. Madden, B. L. Davies, and B. J. Eggleton, "Investigation of all-optical analog-to-digital quantization using a chalcogenide waveguide: A step towards on-chip analog-to-digital conversion," *Opt. Commun.*, vol. 283, no. 10, pp. 2258–2262, 2010.
[28] T. Nagashima, M. Hasegawa, and T. Konishi, "40 GSample/s all-optical analog to digital conversion with resolution degradation prevention," *IEEE Photon. Technol. Lett.*, vol. 29, no. 1, pp. 74–77, 2017.
[29] P. Sethi and S. Roy, "Ultrafast all-optical flip-flops, simultaneous comparator-decoder and reconfigurable logic unit with silicon microring resonator switches," *IEEE J. Sel. Top. Quantum Electron.*, vol. 20, no. 4, pp. 118–125, 2014.
[30] X. Ji *et al.*, "Ultra-low-loss on-chip resonators with sub-milliwatt parametric oscillation threshold," *Optica*, vol. 4, no. 6, pp. 619–624, 2017.